International Journal of Nanomedicine

Dovepress
Taylor & Francis Group

Open Access Full Text Article

ORIGINAL RESEARCH

Targeted Co-Delivery of Curcumin and Astragaloside IV via Hybrid Membrane-Coated Biomimetic Liposomes for Enhanced Lung Cancer Therapy

Hongmei Liu[1,*], Liangliang Lv[1,2,*], Shangqin Yang[1,*], Mingjie Peng[1,3], Kerong Tu[1], Yanheng Wu[1], Lulu Cai[1]

[1]Department of Pharmacy, Personalized Drug Research and Therapy Key Laboratory of Sichuan Province, Sichuan Provincial People's Hospital, University of Electronic Science and Technology of China, Chengdu, People's Republic of China; [2]Department of Pharmacy, Yuechi County People's Hospital, Guangan, People's Republic of China; [3]School of Pharmacy, Chengdu University, Chengdu, People's Republic of China

*These authors contributed equally to this work

Correspondence: Lulu Cai, Department of Pharmacy, Personalized Drug Research and Therapy Key Laboratory of Sichuan Province, Sichuan Provincial People's Hospital, University of Electronic Science and Technology of China, Chengdu, 610072, People's Republic of China, Email cailulu@med.uestc.edu.cn

Background: Lung cancer is the malignant tumor with the highest incidence and lethality worldwide. Existing therapeutic modalities suffer from side effects, drug resistance, and limited efficacy, and there is an urgent need to develop safer and more effective therapeutic strategies. Curcumin (Cur) and astragaloside IV (AS) are promising natural anti-cancer agents. However, their poor aqueous solubility and low bioavailability limit their clinical efficacy. Natural cell membrane-based biomimetic drug delivery platform provides an effective strategy for efficient and targeted co-administration.

Methods: The optimal synergistic ratio of Cur and AS against lung cancer cells was determined using the Combination Index (CI) method. Dual-drug-loaded liposomes were prepared via the thin-film hydration method and subsequently coated with a hybrid membrane derived from cancer cells and erythrocytes to form biomimetic liposomes (CM@AC lip). These nanoparticles were characterized for size, charge, stability, and drug release. Their targeting, endocytosis mechanism, antitumor efficacy, and biosafety were evaluated in vitro and in vivo.

Results: The CM@AC liposomes exhibited a uniform spherical structure with a synergistic ratio of 1.5:1 for AS and Cur. The liposomes had a particle size of 111.86 ± 4.12 nm, a Zeta potential of −20.8 ± 3.63 mV, and encapsulation efficiencies of 63.81 ± 1.22% for Cur and 60.38 ± 0.89% for AS, respectively. The liposomes demonstrated excellent stability. Cellular and animal studies confirmed its superior tumor-targeting ability and immune evasion. CM@AC lip significantly enhanced cytotoxicity, apoptosis, and invasion inhibition against Lewis lung carcinoma cells compared to single-drug treatments. In vivo, it achieved a high tumor inhibition rate (74.59 ± 17.52%) without inducing significant systemic toxicity.

Conclusion: The hybrid membrane-coated biomimetic liposome effectively co-delivers Cur and AS-IV, demonstrating enhanced antitumor efficacy and favorable biosafety via synergistic action, improved targeting, and immune evasion. This strategy presents a promising platform for lung cancer combination therapy.

Keywords: lung cancer, curcumin, astragaloside IV, biomimetic liposomes, targeted delivery

Introduction

Lung cancer is the cancer with the highest incidence and mortality rate in the world, seriously threatening human health and survival.[1,2] Clinical treatments for lung cancer mainly include surgery, radiotherapy, immunotherapy and targeted therapy.[3–5] However, surgery is suitable to early-stage patients and carries a high risk of recurrence;[6] radiotherapy is

https://doi.org/10.2147/IJN.S558285
Received: 4 August 2025
Accepted: 22 December 2025
Published: 14 January 2026

associated with severe toxicity and potential resistance;[7] targeted therapies struggle to overcome tumor heterogeneity;[8] the emerging immunotherapy shows low response rates and can induce immune-related adverse events.[9,10] These limitations underscore the urgent need for more effective and safer therapeutic approaches for lung cancer.

Curcumin, a natural polyphenolic compound extracted from the rhizome of *Curcuma longa*, has demonstrated significant anti-lung cancer activity through various mechanisms, such as inhibiting invasion and metastasis, promoting apoptosis, and suppressing angiogenesis.[11,12] In addition, curcumin can also reverse the resistance and enhance the efficacy of chemotherapeutic agents,[13,14] and has been classified as a third-generation cancer chemopreventive drug by the National Cancer Institute (NCI) of the United States.[15] It also possesses a high safety profile and is recognized as "Generally Recognized As Safe" (GRAS) by the FDA,[16] further highlighting its therapeutic potential in lung cancer. Astragaloside IV, a bioactive compound isolated from *Astragalus membranaceus*, is derived from a herb widely used in Asian traditional medicine, particularly for the treatment of cancer.[17,18] Recent studies have shown that astragaloside inhibits the growth of tumor cells and enhances the function of the body's immune system by regulating multiple signaling pathways,[19,20] and exerts anti-lung cancer effects. Although both curcumin and astragaloside exhibit promising anticancer effects when applied individually, their efficacy is often limited by the complexity and heterogeneity of tumors.[21,22] Combination therapy that targets multiple pathways and molecular mechanisms offers a rational strategy to achieve synergistic effects.[23,24] Therefore, co-delivery of curcumin and astragaloside represents a promising approach for enhanced anti-lung cancer efficacy.

Unfortunately, both curcumin and astragaloside suffer from poor aqueous solubility, low bioavailability, as well as rapid metabolism and clearance in vivo.[25,26] To overcome the limitations of curcumin and astragaloside, and to fully harness their anticancer potential, it is critical to develop an advanced drug delivery system that improves solubility, stability, and tumor-specific targeting.[27–29] Liposomes have been extensively investigated as versatile nanocarriers due to their high biocompatibility, and ability to encapsulate both hydrophilic and hydrophobic drugs. However, conventional liposomes often face challenges such as rapid clearance by the reticuloendothelial system (RES), limited circulation time, and insufficient tumor accumulation. To address these issues, biomimetic nanoparticles, which integrate nanocarriers with natural cell-derived membranes, have recently gained increasing attention.[30,31] These systems imitate the biological characteristics of natural cells—such as self-recognition, immune evasion, and homotypic adhesion—thus providing superior pharmacokinetics and enhanced tumor targeting. Among them, cancer cell membrane-coated nanoparticles exhibit homologous targeting ability that promotes specific accumulation in tumors, while erythrocyte membrane-coated nanoparticles prolong blood circulation by avoiding immune clearance.[32,33] Therefore, hybrid membrane-modified liposomes that combine the two types of membranes can simultaneously achieve long circulation, immune escape, and tumor-specific targeting.

In this study, we developed a hybrid membrane-camouflaged liposome (CM@AC Lip), co-loaded with curcumin and astragaloside, to explore its therapeutic potential in lung cancer. The optimal drug combination ratio was first identified based on synergistic anti-tumor effects. The dual-drug-loaded liposomes were then functionalized with hybrid membranes derived from lung cancer cells and erythrocytes. We systematically investigated the physicochemical characteristics, targeting, anticancer activity, and biosafety of this formulation in both in vitro and in vivo models, aiming to establish a novel combination drug strategy and candidate formulation for lung cancer treatment (Figure 1).

Materials and Methods

Materials

Curcumin (purity ≥ 99%) and astragaloside IV (purity ≥ 99%) were obtained from Manster Biotechnology Co.,Ltd (Chengdu, China). Soybean lecithin and DSPE-PEG_{2000} were purchased from Aladdin Chemistry Co. Ltd (Shanghai, China). Cholesterol was acquired from Avitol Pharmaceutical Technology Co. Ltd (Shanghai, China). Indocyanine green was purchased from Apexbio (USA). Tris-Glycine SDS-PAGE electrophoresis buffer was purchased from Sevier Biotechnology (Chengdu, China). DAPI staining solution was purchased from Solebaum Biotechnology Co (Beijing, China). One-step PAGE gel rapid preparation kit (10%) purchased from Yase Biomedical Technology Co (Shanghai, China). The Tunel kit was purchased from Wuhan Snow Pigeon Biotechnology Co (Wuhan China). DAB color

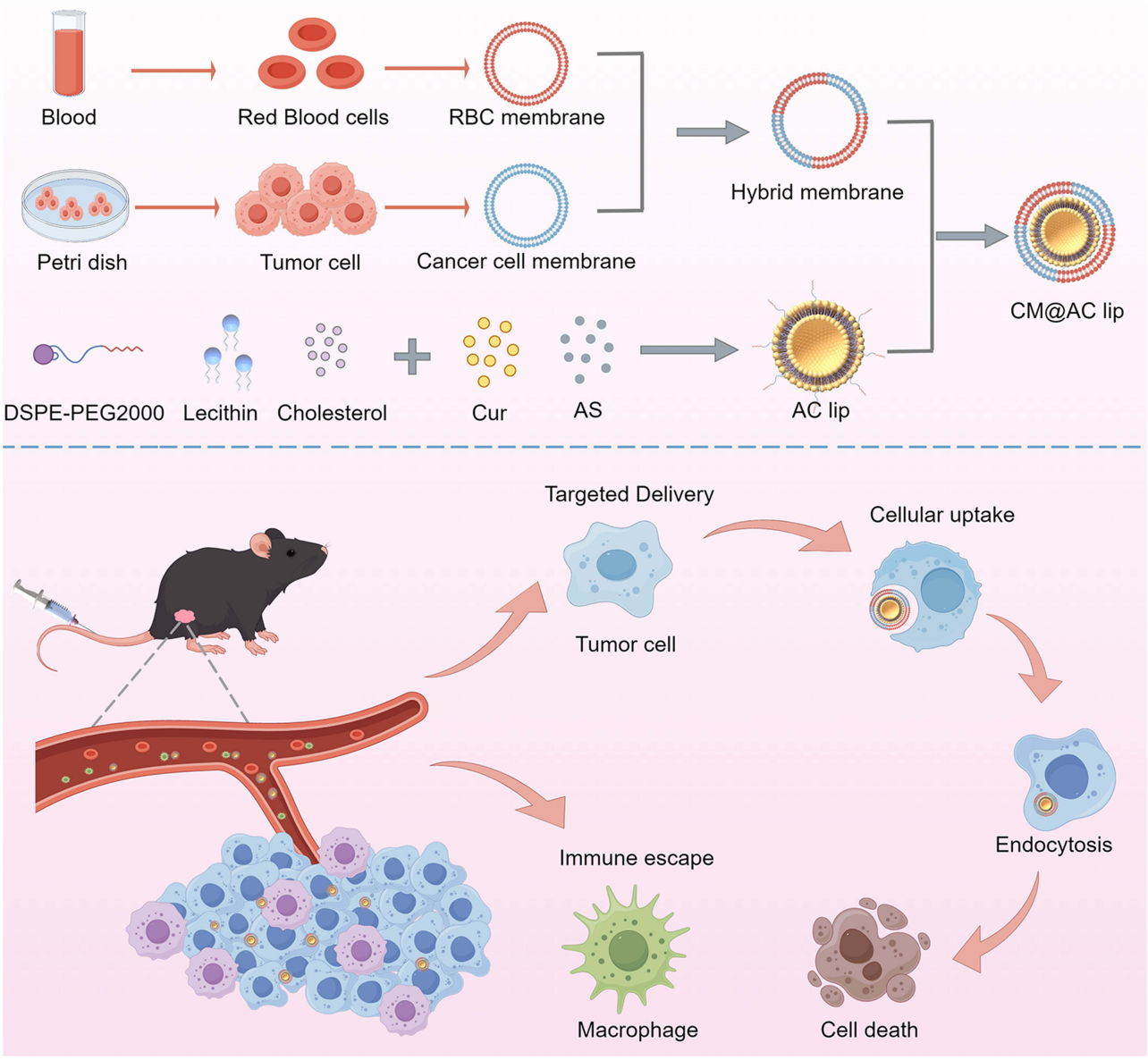

Figure 1 Schematic illustration of CM@AC liposome-mediated lung cancer treatment. Figure created with Figdraw (https://www.figdraw.com).

development kit (DAB4033) was purchased from Novozymes Biotechnology Co (Nanjing, China). Ethanol was purchased from Windship Chemical Reagent Technology Co. Ltd (Tianjin, China).

LLC (Lewis lung carcinoma) cells and RAW264.7 cells were purchased by Punosai Life Sciences Co. Ltd (Wuhan, China). Cells were maintained in Dulbecco's Modified Eagle's Medium (DMEM, Gibco, USA) supplemented with 10% fetal bovine serum (FBS, Gibco, USA), 1% penicillin (100 U/mL), and 1% streptomycin (100 μg/mL), and incubated at 37 °C in a humidified atmosphere containing 5% CO_2.

Female BALB/c mice (18–20 g) purchased from Chengdu Mouse Daqiang Biotechnology Co. (License number: SYXK (Chuan) 2023–0058) and housed under the SPF conditions at the Institute of Experimental Animals, Sichuan Provincial People's Hospital. Animals were maintained under controlled environmental conditions (23 ± 2 °C, 55 ± 10% relative humidity) with free access to food and water for one week prior to experiments. All procedures involving animals were conducted in accordance with the Guidelines for the Care and Use of Laboratory Animals and in compliance with the ARRIVE guidelines, with approval from the Animal Care and Use Committee of Sichuan Provincial People's Hospital (ethical approval number: 2024–91).

https://doi.org/10.2147/IJN.S558285

Synergy Analysis Using SynergyFinder

LLC cells were seeded into 96-well plates (5×10^3 cells/well) and treated with various concentrations of curcumin (0, 40, 60, 80, 120, 160, 200, 240 μM) in combination with astragaloside (0, 40, 60, 80, 120, 160, 200, 240, 320, 480, 600, 640 μM). Cell viability was assessed using the CCK-8 assay. Drug synergy was quantified using SynergyFinder software (https://synergy-finder.fimm.fi), and drug combination response heatmaps were generated. The combination index (CI) was also calculated using CalcuSyn software, with CI < 1 indicating synergy, CI = 1 indicating additivity, and CI > 1 indicating antagonism.

Preparation of Curcumin-Astragaloside Co-Loaded Liposomes (AC Lip)

AC liposomes were prepared using a thin-film hydration method. Briefly, curcumin, astragaloside, lecithin, cholesterol, and DSPE-PEG_{2000} were mixed at a drug-to-lipid molar ratio of 1:15 and a phospholipid-to-cholesterol molar ratio of 4:1. The components were dissolved in 12 mL of ethanol. The solvent was then evaporated using a rotary evaporator at 37 °C to form a thin lipid film. The film was hydrated with 5 mL of phosphate-buffered saline (PBS, pH 7.4) at 37 °C for 30 min. The hydrated solution was probe-sonicated on ice for 5 min (195 W, 5 s on / 1 s off). The liposomal dispersion was sequentially extruded through 0.45 μm and 0.22 μm polycarbonate membranes to obtain uniform AC liposomes.

Extraction and Purification of Cell Membranes

Extraction of erythrocyte membrane: Whole blood was collected from the abdominal aorta of rats into anticoagulant tubes and centrifuged at 20000 g for 10 min at 4 °C to separate erythrocytes. The plasma was discarded, and erythrocytes were washed three times with PBS. The erythrocytes were then lysed in a hypotonic buffer (10 mM Tris-HCl, pH 7.4) on ice for 30 min and centrifuged at 20000 g for 20 min. The precipitate was washed with hypertonic buffer (10 mM Tris-HCl, 1 mM EDTA, pH 7.4) on ice for 30 min, centrifuged again, and resuspended in PBS. After three additional washes, purified erythrocyte membranes were collected and stored at –80 °C.

Extraction of cancer cell membranes: LLC cells in logarithmic growth phase were collected by trypsinization and centrifuged at 1000 g for 5 min at 4 °C. The cell pellet was washed three times with cold PBS and resuspended in hypotonic buffer (10 mM Tris-HCl, pH 7.4), followed by incubation on ice for 30 min. The lysate was centrifuged at 1000 g for 10 min to remove nuclei and debris, and the supernatant was collected. The supernatant was mixed with hypertonic buffer (10 mM Tris-HCl, 1 mM EDTA, pH 7.4), incubated on ice for another 30 min, and centrifuged at 20000 g for 20 min to obtain membrane. The cancer membrane was washed three times with PBS and stored at −80 °C.

Preparation of CM@AC Lip

To prepare the biomimetic liposomes, hybrid membranes derived from erythrocytes and cancer cells were fused onto AC liposomes via probe sonication. Specifically, erythrocyte membranes and cancer cell membranes were mixed at a ratio of 2:1 membrane protein and fused by ultrasonic probe (65 W, 3 s on / 2 s off, 5 min). And then, hybrid membranes were mixed with AC liposomes at a mass ratio of erythrocyte membrane to curcumin of 1:2. The mixture was sonicated using an ultrasonic probe (65 W, 3 s on / 2 s off, 5 min) to facilitate membrane coating, named CM@AC lip.

Particle Size, Zeta Potential, Morphology, and Stability of CM@AC Lip

The morphology of CM@AC lip was visualized via the transmission electron microscope (TEM). The particle size distribution and zeta potential were measured using a Litesizer™ 500 nanoparticle and zeta potential Analyzer. CM@AC lip was placed at 4 °C, and the initial stability was evaluated by measuring changes in particle size over the course of one month.

Drug Loading Capacity and Encapsulation Efficiency of CM@AC Lip

A certain volume of liposomal suspension was mixed with methanol to disrupt the liposome structure and release the encapsulated drugs. The mixture was vortexed and centrifuged at 12000 rpm for 3 minutes. The supernatant was collected and analyzed by high-performance liquid chromatography (HPLC). Drug concentrations were quantified

based on standard curves for curcumin and astragaloside. Encapsulation efficiency (EE%) and Drug Loading Capacity (DL%) was calculated using the following formula:

$$\mathrm{EE\%} = (W_{loaded}/W_{total}) \times 100\%,\ \mathrm{DL} = (W_{loaded}/W_{all}) \times 100\%$$

In the formulas, W_{loaded} represents the amount of drug in the liposome after removal of free drug, W_{total} refers to the total amount of drug initially added, and W_{all} is the total amount of carrier and drug.

Membrane Protein Analysis of CM@AC Lip

To confirm successful membrane coating, protein profiles of raw erythrocyte membranes (RCM), tumor cell membranes (TCM), AC liposomes, and CM@AC liposomes were compared via SDS-PAGE analysis. Each sample was lysed with 200 μL of RIPA buffer, followed by probe sonication on ice (65 W, 1 min). After centrifugation (4 °C, 15 min), the supernatants were collected, mixed with 5× loading buffer at a ratio of 4:1 (v/v), and denatured at 100 °C for 10 min. Samples (10 μL per well) were loaded onto 10% SDS-PAGE gels and electrophoresed at 90 V for 30 min, then at 120 V for an additional hour. The gels were stained with Coomassie Brilliant Blue for 5 h, destained, and imaged using a gel documentation system to visualize protein band patterns.

FT-IR Detection of CM@AC Lip

CM@AC liposomes were lyophilized to obtain a dry powder. Approximately 1–2 mg of the sample was thoroughly ground with 100–200 mg of potassium bromide (KBr), and the mixture was compressed into a translucent pellet. The spectra of curcumin, astragaloside, blank liposomes, and CM@AC liposomes were recorded using an FT-IR spectrometer after background scanning.

In vitro Drug Release Behavior

The in vitro release behavior of CM@AC lip was assessed using the dialysis method. Briefly, 1 mL of CM@AC liposomes was placed into dialysis bags (MWCO: 1,000 kDa), which were immersed in 10 mL of PBS containing 2% Tween 80 (pH 7.4) and incubated at 37 °C under agitation (100 rpm). At predetermined time points, 1 mL of the release medium was withdrawn and replaced with an equal volume of fresh medium. The concentrations of curcumin and astragaloside in the release medium were quantified by HPLC. All measurements were performed in triplicate.

Mechanisms of Cellular Uptake and Endocytosis

For cellular uptake, LLC and RAW264.7 cells were seeded in 12-well plates at a density of 2×10^5 cells/well. After cell attachment, liposomal formulations containing curcumin were administered. At designated time points, cells were harvested, washed thoroughly with phosphate-buffered saline (PBS) to remove excess extracellular fluorescence, and resuspended in PBS for analysis by flow cytometry. For qualitative visual analysis, after 4 h of incubation, cells were washed twice with cold PBS and fixed with 0.5 mL of tissue fixative for 15 min. After fixation, cells were washed again with PBS, and 1 mL of DAPI solution (1 μg/mL) was added to each well for 10 min to stain the nuclei. Following two additional PBS washes, intracellular fluorescence was observed and recorded using a fluorescence microscope.

For endocytosis analysis, LLC cells were seeded in 12-well plates at a density of 2×10^5 cells/well. After cell attachment, cells were pretreated for 1 h with specific endocytic inhibitors, including chlorpromazine (30 μM), genistein (35 μM), or wortmannin (1 μM), to block clathrin-mediated, caveolae-mediated, and macropinocytosis pathways, respectively. Following inhibitor treatment, DiI-labeled liposomal formulations were added. At the designated time point, cells were collected, thoroughly washed with cold PBS to remove unbound DiI, and resuspended in PBS for flow cytometric analysis. For fluorescence microscopy, the visualization procedure was performed in the same manner as described in the cellular uptake study.

In vitro Cytotoxicity Assay

LLC cells were seeded in 96-well plates at densities of 5×10^3 cells/well. After 24 h of adherence, the culture medium was replaced with medium containing different formulations at various concentrations. Cell viability was assessed at

24 h and 48 h post-treatment using the CCK-8 reagent according to the manufacturer's instructions. Absorbance was measured at 450 nm using a microplate reader.

Transwell Assays for Cell Migration

The migratory capacity of Ishikawa cells was determined using a 24-well Transwell chamber. The Transwell kit was prepared, and the required number of chambers was placed in a 24-well plate. Then, 100 μL of serum-free medium was added to the upper chamber and incubated at 37 °C for 1 h. Cells were resuspended in serum-free medium and counted. The medium was removed carefully, 100 μL of cell suspension (1×10^5 cells/well) was seeded in the upper chamber, and 600 μL of culture medium with 10% FBS and various drugs were added to the lower chamber. Transwell chambers were incubated for 24 h. Nonmigrated cells on the filter side of the upper chamber were removed with a cotton swab. The cells were fixed with 4% paraformaldehyde for 30 min and stained with Giemsa solution. The staining solution was dropped on the lower surface of the chamber to stain transfected cells for 3–5 min. The chambers were washed with 1 × PBS several times and air dried. The field of view was randomly selected, 5 photos at 200 × were taken from each chamber, and the migrated cells were counted.

Apoptosis Assay

LLC cells were seeded in 12-well plates at a density of 2×10^5 cells/well. After cell adhesion, cells were treated with different formulations and incubated for 24 h. Subsequently, cells were harvested, washed with PBS, and stained with Annexin V-FITC and propidium iodide (PI) using a commercial apoptosis detection kit, following the manufacturer's protocol. The proportion of apoptotic cells was analyzed using flow cytometry.

In vivo Pharmacodynamic Evaluation of CM@AC Lip

LLC cells were harvested and suspended in serum-free DMEM at a concentration of 1×10^7 cells/mL. Each mouse was subcutaneously injected with 0.2 mL of the cell suspension into the dorsal region. When the tumor volume reached approximately 100 mm^3, the mice were randomly divided into four groups: PBS, AS (6 mg/kg), Cur (2 mg/kg), and CM@AC lip (equivalent to 2 mg/kg Cur). Treatments were administered via tail vein injection every other day. Tumor volumes and body weights were recorded every other day throughout the treatment period. After 16 days, the mice were euthanized, and tumors were excised and weighed. Major organs including heart, liver, spleen, lungs, and kidneys were collected for histological analysis to assess potential systemic toxicity associated with the treatments. The tumor growth inhibition (TGI) rate was calculated using the formula:

$$\mathrm{TGI} = \left[1 - RTV_{test}/RTV_{Control}\right] * 100\%$$

Where RTV_{test} is the relative tumor volume of the experimental group and RTV_{control} is the relative tumor volume of the control group ($RTV{=}V_t/V_0$), with V_0 being the initial tumor volume and V_t the tumor volume at the endpoint.

In vivo Targeting Distribution of CM@AC Lip

Tumor-bearing mice (tumor volume ~200 mm^3) were randomly assigned into three groups and administered via tail vein injection with free ICG, ICG lip, or CM@ICG lip. In vivo fluorescence imaging was conducted at 1, 2, 4, 6, 8, 10, 24, 48, and 72 h post-injection using IVIS spectrum imaging system under 2% isoflurane anesthesia. At 10 h post-injection, mice were euthanized and their major organs (heart, liver, spleen, lung, kidney) and tumor tissues were obtained for in vitro fluorescence imaging.

Biocompatibility

HUVECs were seeded into 96-well plates at a density of 5×10^3 cells per well and allowed to adhere for 24 hours. Subsequently, the cells were treated with blank liposomes at varying concentrations (0, 4, 8, 16, 32, 64, and 128 μM, based on cholesterol content). After 24, 48, and 72 hours of incubation, cell viability was assessed using the Cell Counting Kit-8 (CCK-8) assay to evaluate the cytocompatibility of the liposomes.

In vitro Hemolysis Test

Fresh whole blood was collected from healthy mice and anticoagulated with heparin, followed by centrifugation at 1500 rpm for 20 min at 4 °C. The erythrocyte pellet was washed repeatedly with PBS until the supernatant became pale yellow or colorless. The washed erythrocytes were then diluted with PBS to prepare a 2% erythrocyte suspension. Equal volumes of PBS (negative control), deionized water (positive control), AS, Cur, blank liposomes, and CM@AC lip were mixed with the red blood cell suspension and incubated at 37°C for 3 h. After incubation, images of each sample were taken, followed by centrifugation at 1500 rpm for 10 min. The supernatants were collected, and the absorbance at 540 nm was measured using a microplate reader. The hemolysis rate (HR%) was calculated using the following equation:

$$\mathrm{HR\%} = \left(A_{sample} - A_{negative}\right) / \left(A_{positive} - A_{negative}\right) \times 100\%$$

where A_{sample}, A_{negative}, and A_{positive} represent the absorbance values of the sample, PBS (negative control), and deionized water (positive control), respectively.

In vivo Safety Evaluation

At the end of the treatment period, mice were humanely euthanized, and major organs—including the heart, liver, spleen, lungs, and kidneys—were carefully excised. The harvested tissues were immediately fixed in 4% paraformaldehyde, processed by standard paraffin embedding, sectioned, and stained with hematoxylin and eosin (H&E) for histological evaluation.

Statistical Analysis of Data

All experimental data were expressed as mean ± standard deviation (SD). Statistical analyses were performed using GraphPad Prism 9.0 and SPSS 19.0 software. One-way analysis of variance (ANOVA) was employed for group comparisons. A p-value less than 0.05 was considered statistically significant ($^{*}p < 0.05$, $^{**}p < 0.01$, $^{***}p < 0.001$).

Results

Synergy Ratio Screening

The in vitro cytotoxicity assay revealed that Cur and AS displayed varying degrees of inhibitory effects across concentration ranges of 0–240 μM and 0–640 μM, respectively, when treated individually or in combination at specific ratios. Synergistic interactions were evaluated using SynergyFinder, with the results shown in Figure 2A–C. The analysis indicated that Cur and AS displayed additive or synergistic effects within the concentration range of 0–60 μM for Cur and 0–160 μM for AS, the most significant synergistic cytotoxicity was observed when Cur and AS were combined at a molar ratio of 1:1.5. Under this ratio, the combination index (CI) values remained consistently below 1.0 across various concentrations, indicating a significant synergistic interaction (Figure 2D).

Preparation and Characterization of CM@AC Lip

CM@AC liposomes exhibited a uniform and nanoscale particle size distribution, with an average diameter of approximately 111.86 ± 4.12 nm, a low polydispersity index (PDI= 0.25 ± 0.002), and a zeta potential of −20.8 ± 3.63 mV (Figure 3A and B). The morphologies of AC lip and CM@AC lip were observed by TEM. AC lip exhibited uniformly sized spherical like structures, and CM@AC lip could observed a outer circles of the cell membrane (Figure 3C). The long-term stability of CM@AC lip was evaluated by monitoring changes in particle size and zeta potential over 30 days at 4 °C. As shown in Figure 3D, E and S1, the formulations maintained minimal size and zeta potential variation and the PDI was below 0.3, confirming excellent physical stability.

FT-IR spectroscopy was conducted to verify drug encapsulation. AS exhibited a strong O-H stretching vibration peak at 3383.06 cm^{-1} and an ether bond stretching vibration peak within the range of 1000–1200 cm^{-1}. While Cur displayed a C=O stretching vibration peak at 1608.29 cm^{-1}, along with ether bond and phenolic hydroxyl group stretching vibration peaks around 1100 cm^{-1}. Their physical mixture exhibited their respective characteristic peaks. Notably, the FT-IR spectrum of CM@AC liposomes was similar to that of blank liposomes and lacked the distinctive peaks of AS and Cur

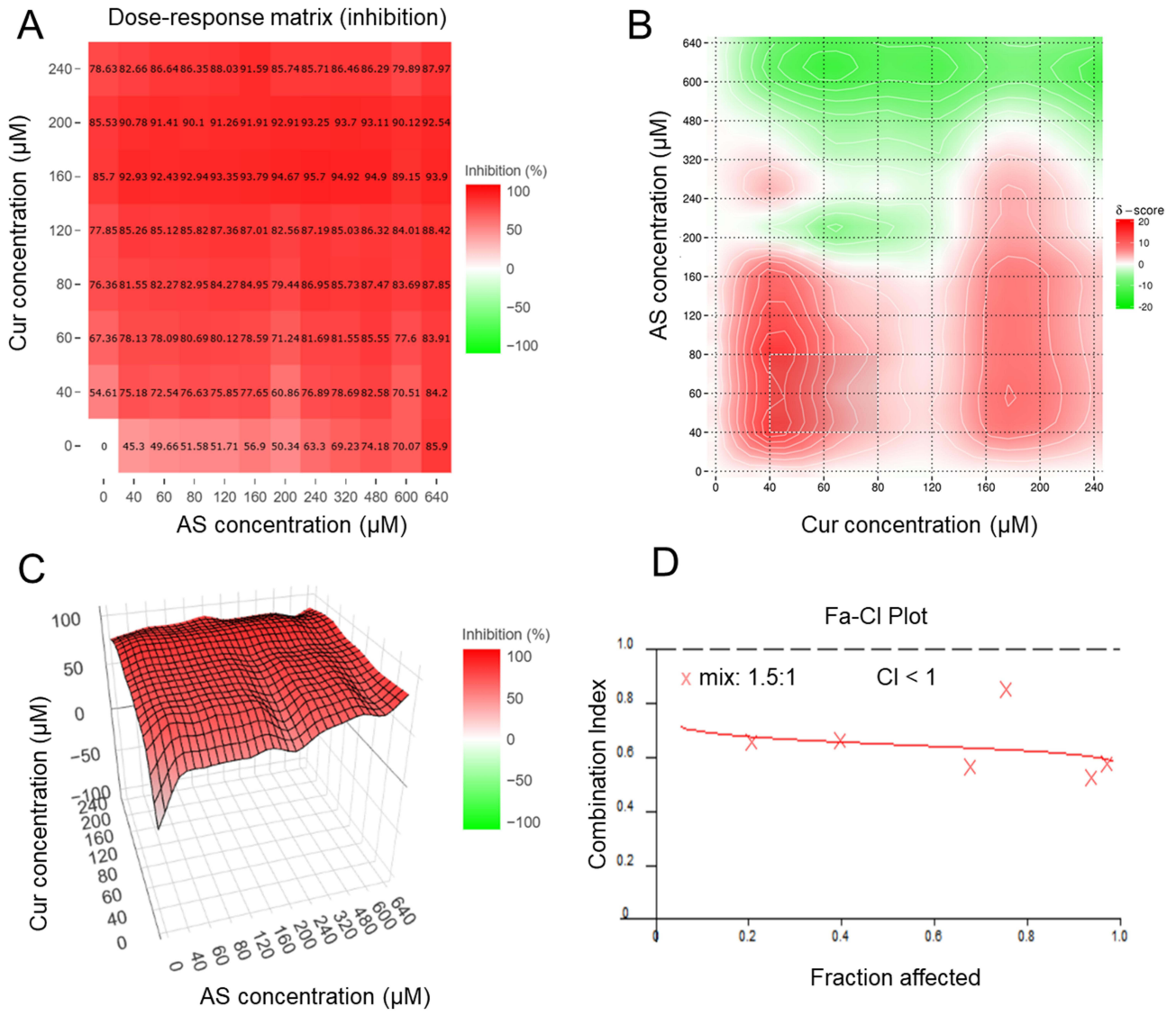

Figure 2 Synergistic ratio screening of curcumin and astragaloside on LLC cells. (**A–C**) Heatmaps of the combinatorial effects of curcumin and astragaloside at various concentrations. (δ-score > 10 represents synergy, −10 ≤ δ-score ≤ +10 represents addition, and δ-score < −10 represents antagonism). (**D**) Combination index–fraction affected (CI–FA) curve of Curcumin and Astragaloside IV combination at a fixed molar ratio of 1.5:1 under different concentrations. All data are presented as mean ± SD (n = 3).

(Figure 3F), suggesting that both drugs were successfully encapsulated. This may be attributed to drug–liposome interactions (eg, hydrogen bonding, hydrophobic effects), which altered the original molecular vibrations of AS and Cur. To verify successful hybrid membrane fusion, protein profile analysis was performed via SDS-PAGE. As shown in Figure 3G, CM@AC lip exhibited protein bands consistent with both RCM and TCM, while uncoated AC liposomes lacked these membrane-specific bands. This confirms the successful membrane coating and suggests potential capabilities for immune evasion and homologous tumor targeting.

Based on the content determination (Figure S2), the encapsulation efficiency of curcumin was 63.81 ± 1.22%, with a drug loading capacity of 5.98 ± 0.04%. For astragaloside IV, the encapsulation efficiency was 60.38 ± 0.89%, and the drug loading capacity was 5.38 ± 0.93%. These results indicate efficient co-encapsulation of both agents into the liposomal formulation, laying a foundation for synergistic drug delivery.

The release profiles of AS and Cur from CM@AC lip were evaluated using a dialysis method under physiological (pH 7.4) and mildly acidic (pH 6.5) conditions. As shown in Figure 3H and I, both drugs exhibited a sustained release pattern over 24 hours. Under physiological conditions, the cumulative release of AS and Cur remained below 40%,

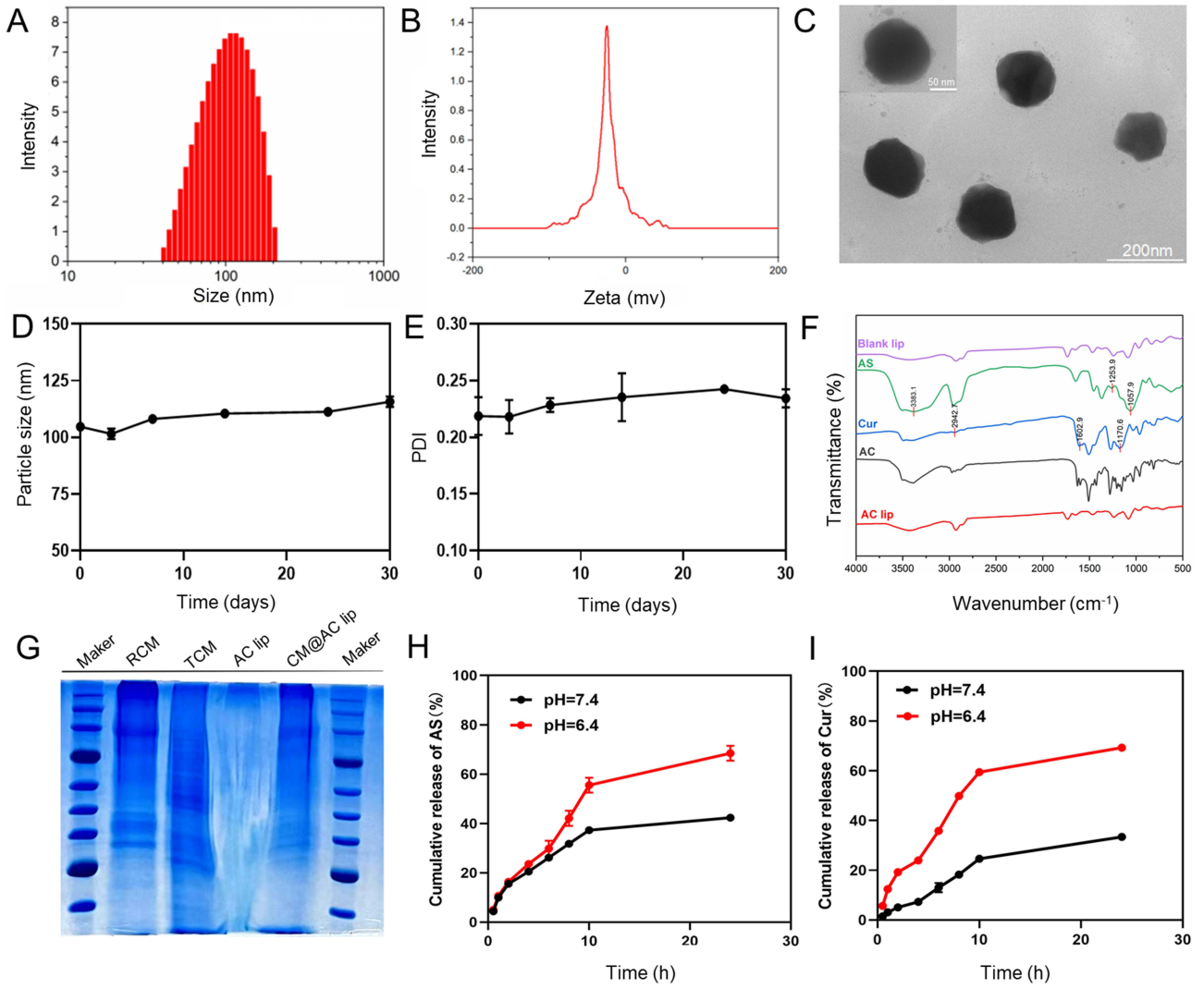

Figure 3 Characterization of CM@AC lip. (**A** and **B**) Particle size and Zeta potential were measured by dynamic light scattering (DLS). (**C**) Transmission electron microscopy (TEM) images of AC lip, scale bar = 200 nm, top left is the TEM image of the CM@AC lip, scale bar = 50 μm. (**D** and **E**) Stability of CM@AC lip. (**F**) FT-IR spectra of CM@AC lip, Cur, AS, and blank lip. (**G**) SDS-PAGE analysis of membrane protein profiles from RCM, TCM, AC lip, and CM@AC lip. (**H** and **I**) In vitro cumulative release profiles of AS and Cur from CM@AC lip at pH 7.4 and pH 6.5. All data are presented as mean ± SD (n = 3).

indicating minimal premature leakage under normal conditions. At pH 6.5, the cumulative release rates increased to 68.48% ± 2.48% for AS and 69.69% ± 1.00% for Cur. This acid-responsive release behavior suggests that CM@AC lip is capable of preferentially releasing their payloads in the acidic tumor microenvironment, potentially enhancing therapeutic efficacy while minimizing systemic side effects.

Immune Escape Ability of CM@AC Lip

Curcumin was employed as a fluorescent tracer to evaluate the immune escape capability of CM@AC liposomes. Cellular uptake by RAW264.7 macrophages was assessed via flow cytometry and fluorescence microscopy. As shown in Figure 4A and B, the uptake of CM@Cur liposomes by RAW264.7 cells was significantly lower than that of both free curcumin and curcumin-loaded liposomes at all measured time. The highest uptake was observed at 6 h, which was selected as the optimal time for subsequent imaging analysis. Fluorescence microscopy (Figure 4C) further confirmed that the CM@Cur group exhibited substantially weaker intracellular fluorescence compared to the other two groups. These findings indicate that the biomimetic membrane coating on CM@AC liposomes effectively reduced phagocytic uptake by macrophages, thereby enhancing their immune evasion capability.

https://doi.org/10.2147/IJN.S558285

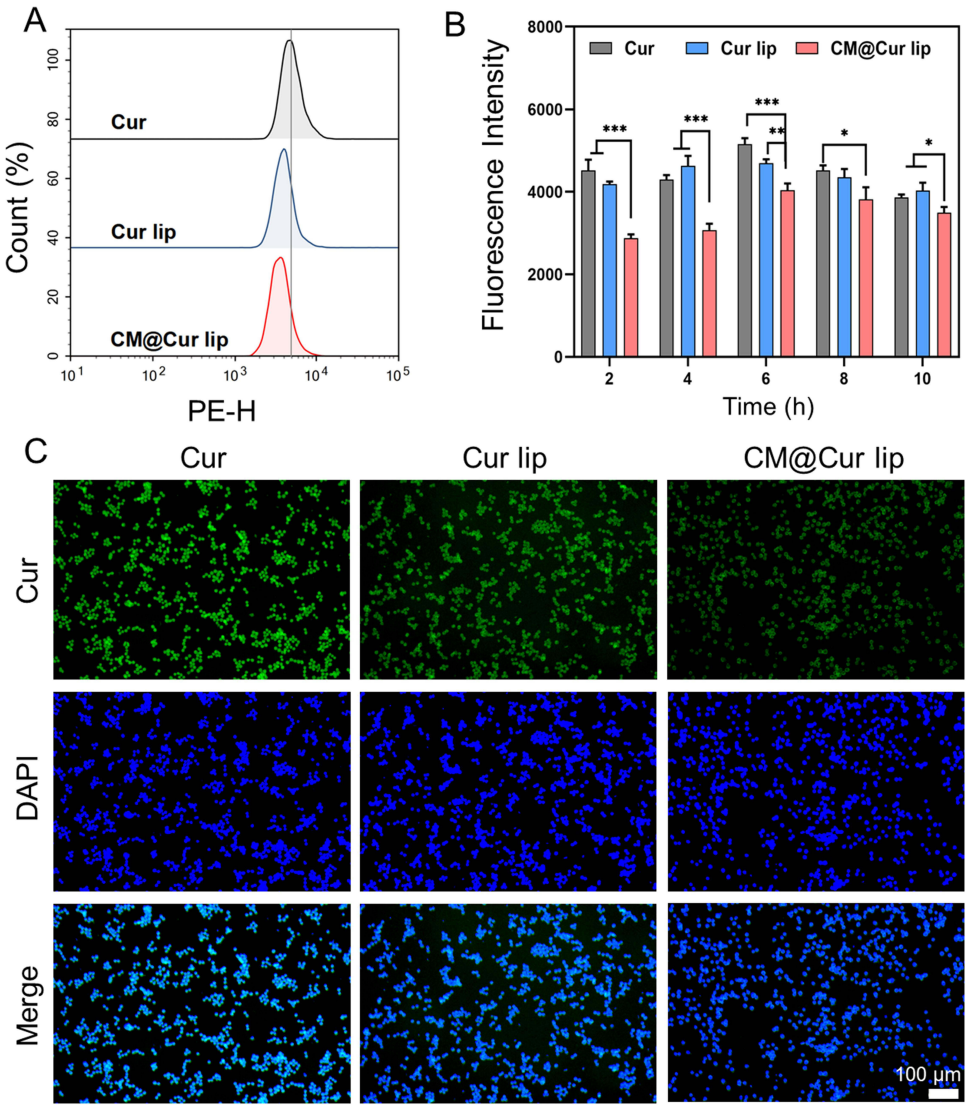

Figure 4 Immune escape ability of CM@AC lip. (**A**) Flow cytometry analysis of RAW264.7 cell uptake of free Cur, Cur lip, and CM@Cur lip. (**B**) Quantitative analysis of fluorescence intensity. (**C**) Fluorescence microscopy images showing intracellular uptake of Cur, Cur lip, and CM@Cur lip by RAW264.7 cells, scale bar = 100 μm. All data are presented as mean ± SD (n = 3). *$p < 0.05$, **$p < 0.01$, ***$p < 0.001$.

Targeted Uptake of CM@AC Liposomes by LLC Cells

The targeting capability of CM@AC liposomes toward Lewis lung carcinoma (LLC) cells was assessed using the membrane-labeled fluorescent dye DiI. Flow cytometry analysis (Figure 5A and B) revealed that CM@DiI liposomes exhibited significantly higher uptake by LLC cells at all time points compared to free DiI and DiI-loaded liposomes (Dil lip). Fluorescence microscopy (Figure 5C) demonstrated markedly stronger red fluorescence intensity in the CM@DiI group, indicating greater cellular internalization. These results confirm that CM@AC liposomes possess enhanced targeting ability toward LLC cells, due to homologous membrane-mediated recognition and uptake.

Mechanistic of Cellular Internalization Pathways

The intracellular transport mechanism of CM@AC liposomes was investigated by analyzing changes in cellular uptake under different inhibitory conditions. Flow cytometry results (Figure 6A and B) revealed that the uptake of CM@AC liposomes by LLC cells was significantly reduced following pretreatment with wortmannin, suggesting that macropinocytosis plays a predominant role in their internalization. Additionally, a marked decrease in cellular uptake was observed when cells were incubated at 4 °C, indicating that the uptake process is energy-dependent. Fluorescence imaging results

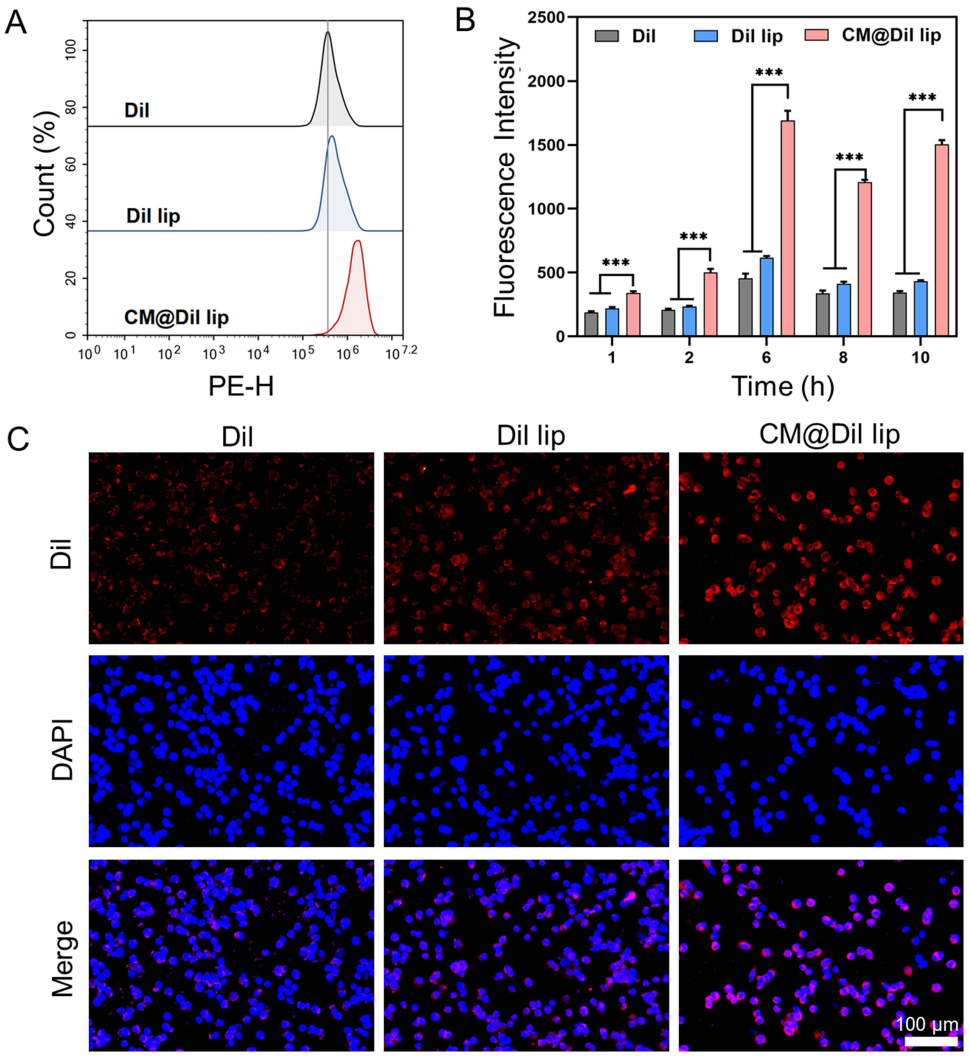

Figure 5 Targeted uptake of CM@AC liposomes by LLC cells. (**A**) Flow cytometry analysis of LLC cell uptake of free Dil, Dil-labeled liposomes, and CM@Dil liposomes. (**B**) Quantitative analysis of fluorescence intensity. (**C**) Fluorescence microscopy images of cellular uptake (scale bar = 50 μm). All data are presented as mean ± SD (n = 3), ***$p < 0.001$.

(Figure 6C) further supported these findings, showing attenuated red fluorescence intensity in LLC cells treated with wortmannin and incubated at 4°C, consistent with the flow cytometry. Collectively, these results demonstrate that the cellular internalization of CM@AC lip is primarily mediated via macropinocytosis in an energy-dependent manner.

In vitro Cytotoxicity

The cytocompatibility of blank liposomes was assessed using HUVECs. As shown in Figure 7A, the liposomes exhibited no significant cytotoxicity across all concentrations and time points. Even at the highest concentrations, cell viability generally remained above 80%, indicating good biocompatibility. These findings suggest that the liposomal formulation is safe for normal endothelial cells and suitable for further in vivo applications. The cytotoxic effects of free AS, Cur, and CM@AC liposomes on LLC cells were shown in Figure 7B–D, LLC cells maintained high viability following treatment with AS for both 24 and 48 hours until a significant cytotoxicity was observed at a concentration of 160 μM (Figure 7B). In contrast, Cur exhibited a more potent inhibitory effect, significantly reducing cell viability at concentrations as low as 40 μM (Figure 7C). Notably, when AS and Cur were co-delivered using hybrid membrane-coated liposomes (CM@AC lip), a markedly enhanced cytotoxic effect was observed (Figure 7D). A549 cells also showed consistent results in cytotoxicity (Figure S3).

https://doi.org/10.2147/IJN.S558285

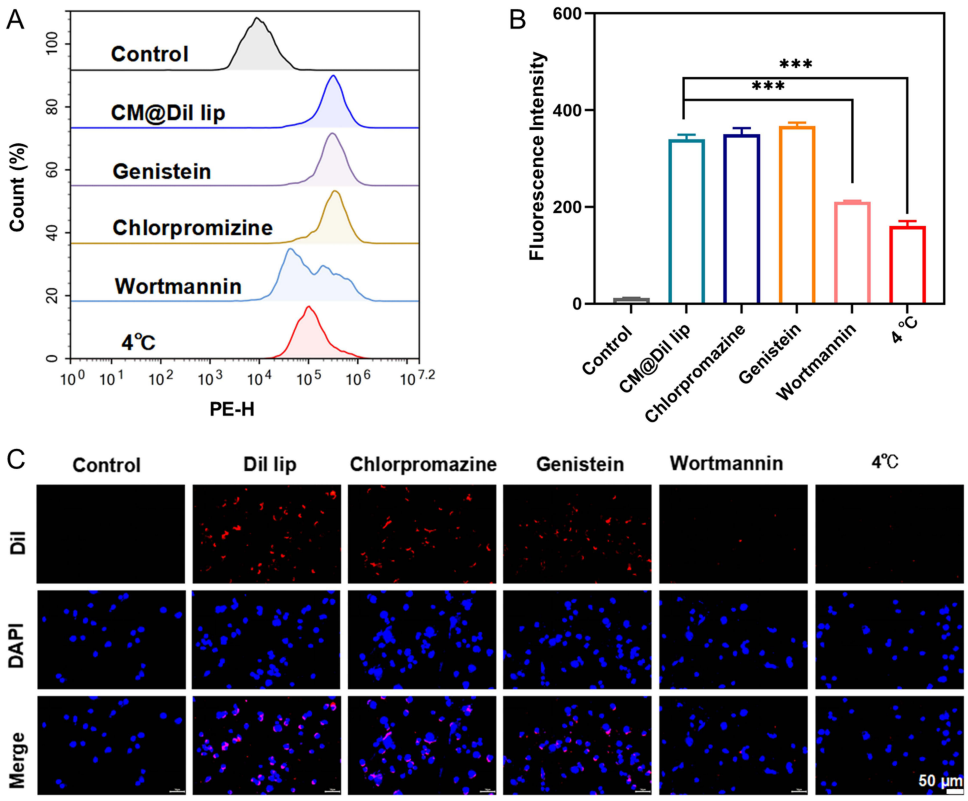

Figure 6 Results of cellular transport mechanisms. (**A**) Flow cytometry analysis of CM@AC lip uptake in LLC cells after treatment with different endocytic inhibitors and low-temperature incubation. (**B**) Quantification of cellular fluorescence intensity based on flow cytometry. (**C**) Fluorescence microscopy images showing cellular uptake under different conditions (scale bar = 50 μm). All data are presented as mean ± SD (n = 3), ***$p < 0.001$.

Cell Apoptosis and Cell Invasion Assay

To evaluate the pro-apoptotic effects of different treatments on LLC cells, Annexin V-FITC/PI staining followed by flow cytometry was performed. As shown in Figures 7E and F, AS and Cur resulted in an increase in total apoptotic rates to 6.79 ± 0.15% and 19.37 ± 0.80%, respectively, compared with 3.00 ± 0.70% in the control group, indicating that both compounds possessed pro-apoptotic activity. Notably, CM@AC liposomes induced a significantly higher apoptosis rate of 23.02 ± 0.30%. These results suggest that the co-delivery of AS and Cur via hybrid membrane-coated liposomes synergistically enhances the induction of apoptosis in LLC cells.

The effects of different formulations on the invasive ability of LLC cells were assessed using transwell assays. As shown in Figure 7G and H, CM@AC liposomes significantly suppressed LLC cell invasion compared to all other groups. These results suggest that the co-delivery of AS and Cur in CM@AC liposomes has the potential to effectively suppress lung cancer metastasis.

In vivo Biodistribution

To evaluate the tumor targeting of the liposome formulation, the nanoparticles were labeled with the indocyanine green (ICG). Free ICG, ICG-loaded liposomes (ICG lip), and hybrid cell membrane-coated ICG liposomes (CM@ICG lip) were intravenously injected into BALB/c mice bearing LLC tumors, and real-time tissue distribution was monitored using an IVIS spectral imaging system. As shown in Figures 8A and B, free ICG exhibited rapid clearance and weak fluorescence, which substantially diminished after 6 hours post-injection. In contrast, mice treated with ICG liposomes showed stronger fluorescence accumulation at the tumor, primarily due to the enhanced permeability and retention (EPR) effect. Notably, CM@ICG liposomes exhibited the strongest tumor fluorescence signal, maintaining persistent intensity even at 10 hours post-injection, by which time fluorescence in the other groups had essentially disappeared. Ex vivo imaging of excised organs and tumors further

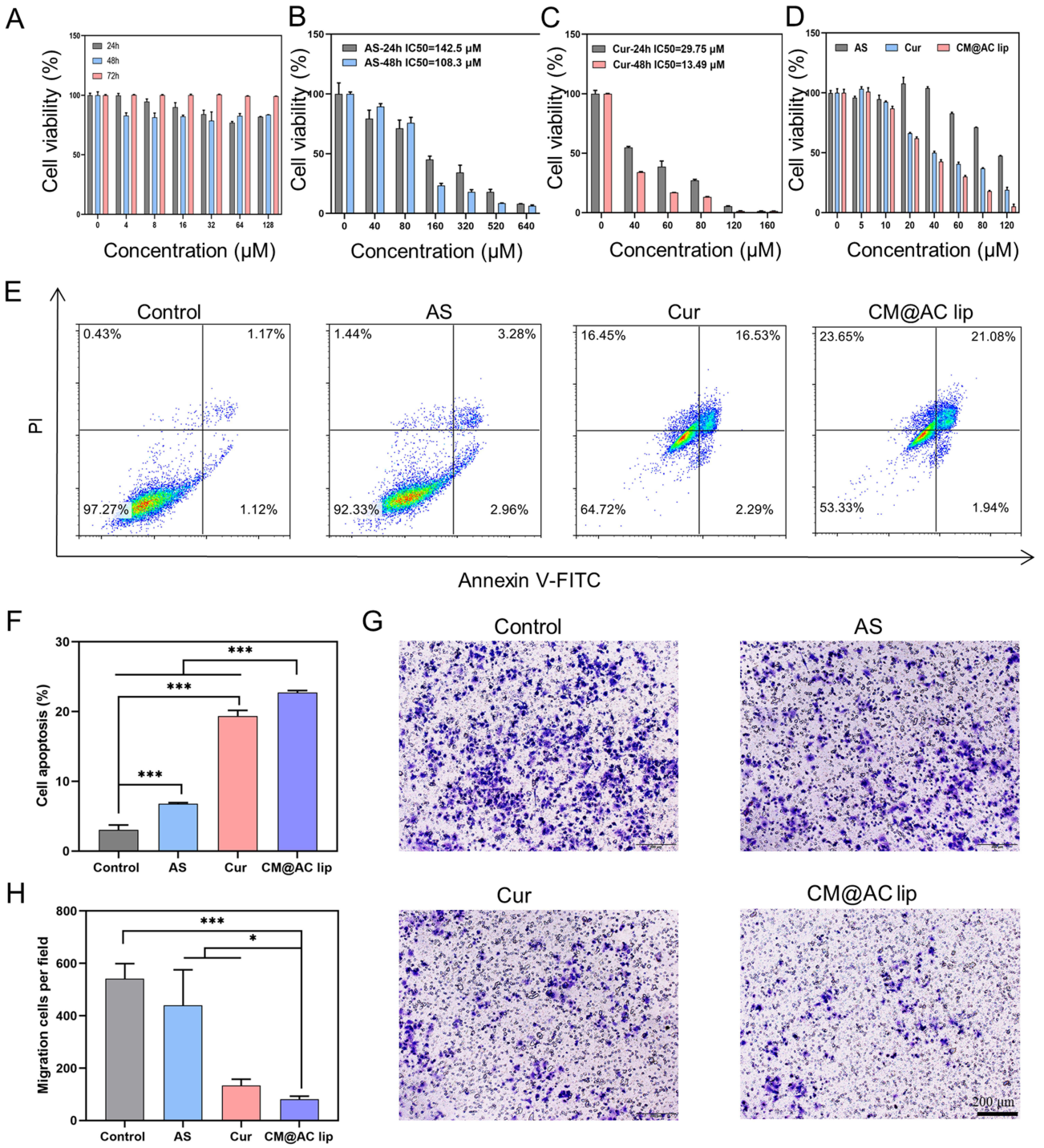

Figure 7 In vitro biocompatibility, cytotoxicity, apoptosis, and invasion inhibition in LLC cells. (**A**) Vector biocompatibility. (**B** and **C**) Cytotoxicity of AS and Cur at different concentrations after 24 h and 48 h treatment. (**D**) Cytotoxicity of different groups on LLC cells. (**E**) Apoptosis analysis of LLC cells after 24 h of treatment. (**F**) Quantification of apoptotic rates based on flow cytometry. (**G**) Representative images of transwell assay after 24 h of treatment (scale bar = 200 μm). (**H**) Quantification of migrated LLC cells. All data are presented as mean ± SD (n = 3). *$p < 0.05$, ***$p < 0.001$.

confirmed these findings (Figures 8C and D). Compared with the free ICG and ICG liposome groups, the CM@ICG liposome group demonstrated significantly stronger fluorescence intensity in the tumor tissues, supporting their enhanced tumor-targeting capability.

https://doi.org/10.2147/IJN.S558285

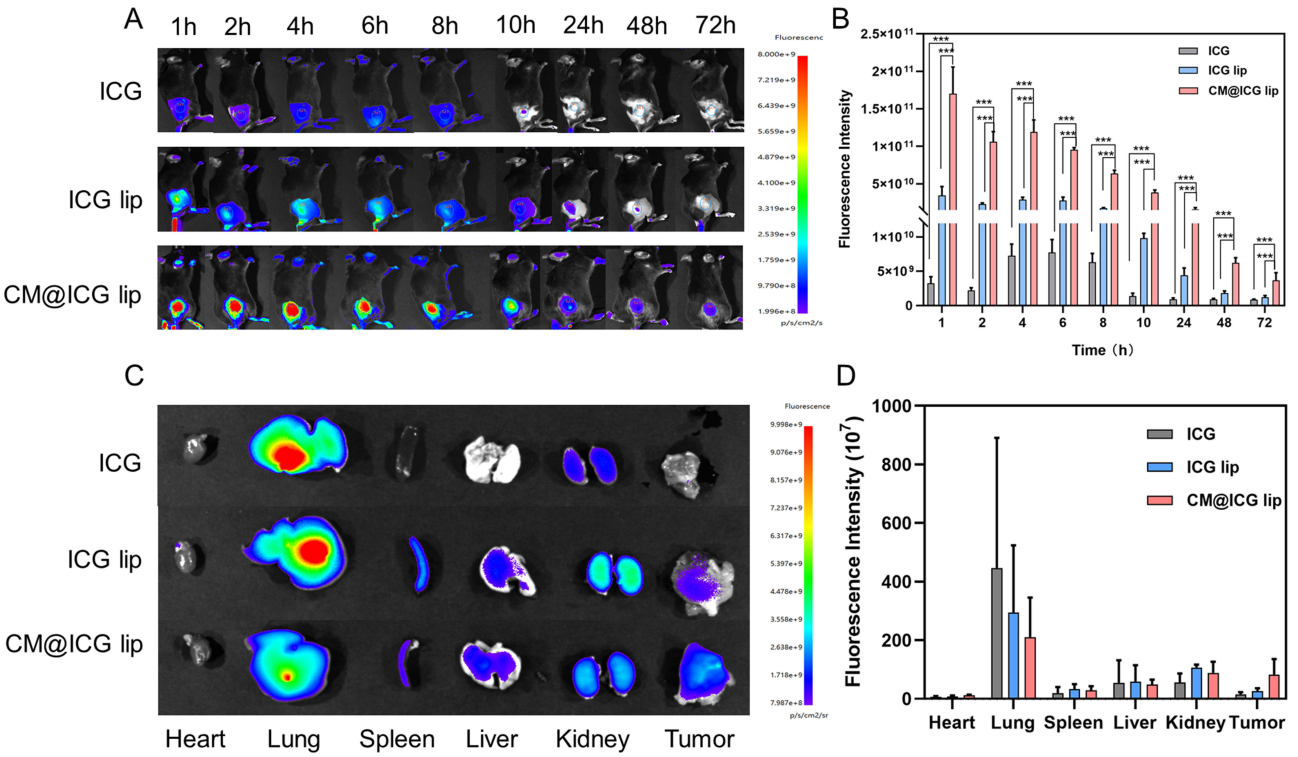

Figure 8 In vivo biodistribution of different ICG formulations in LLC tumor-bearing mice. (**A** and **B**) Representative fluorescence images and quantitative analysis of free ICG, ICG lip, and CM@ICG lip at various time points post-injection. (**C**) Ex vivo fluorescence images of major organs and tumors 10 hours after injection. (**D**) Quantitative fluorescence intensity of excised organs and tumors. All data are presented as mean ± SD (n = 3), ***$p < 0.001$.

In vivo Antitumor Efficacy of CM@AC Lip

To assess the antitumor efficacy of CM@AC liposomes, LLC tumor-bearing mice were intravenously injected with saline (Control), AS, Cur, or CM@AC lip (Figure 9A). Tumor growth and tumor weight (Figure 9B–D, 9F) revealed rapid tumor progression in both the Control and AS groups. In contrast, tumor growth was significantly inhibited in the Cur and CM@AC lip groups, with CM@AC lip demonstrating the most potent suppression. Specifically, the tumor growth inhibition (TGI) rate for the AS group was 22.4%, showing no significant difference from the control. The Cur group exhibited a TGI of 31.9%, while the CM@AC lip achieved the highest therapeutic efficacy, with a TGI rate of 74.6%. Throughout the 14-day treatment period, all groups maintained stable body weight (Figure 9E), suggesting good systemic tolerance and minimal toxicity. To further investigate the anti-proliferative and pro-apoptotic effects in vivo, tumor tissue were subjected to Ki67 and TUNEL immunofluorescence staining. As shown in Figure 9G, Ki67-positive cell populations were markedly reduced in all treatment groups, with the CM@AC lip showing the lowest expression. TUNEL-positive apoptotic cells were significantly elevated in the CM@AC lip group compared to monotherapy groups (Figure 9H), confirming dual suppression of proliferation and induction of apoptosis.

In vivo Biosafety Evaluation

The hemocompatibility of CM@AC lip was assessed via hemolysis testing. As illustrated in Figures 10A and B, AS, and CM@AC lip exhibited minimal hemolytic activity, comparable to the negative control (saline). Although a slight increase in hemolysis was observed in the Cur group, the rate remained below 5%, which is within the acceptable safety threshold. In addition, Histopathological examination of major organs (heart, liver, spleen, lungs, and kidneys) via H&E staining (Figure 10C) revealed no evident tissue damage or pathological abnormalities in any group. These findings confirm the favorable biosafety and biocompatibility of CM@AC liposomes for in vivo applications.

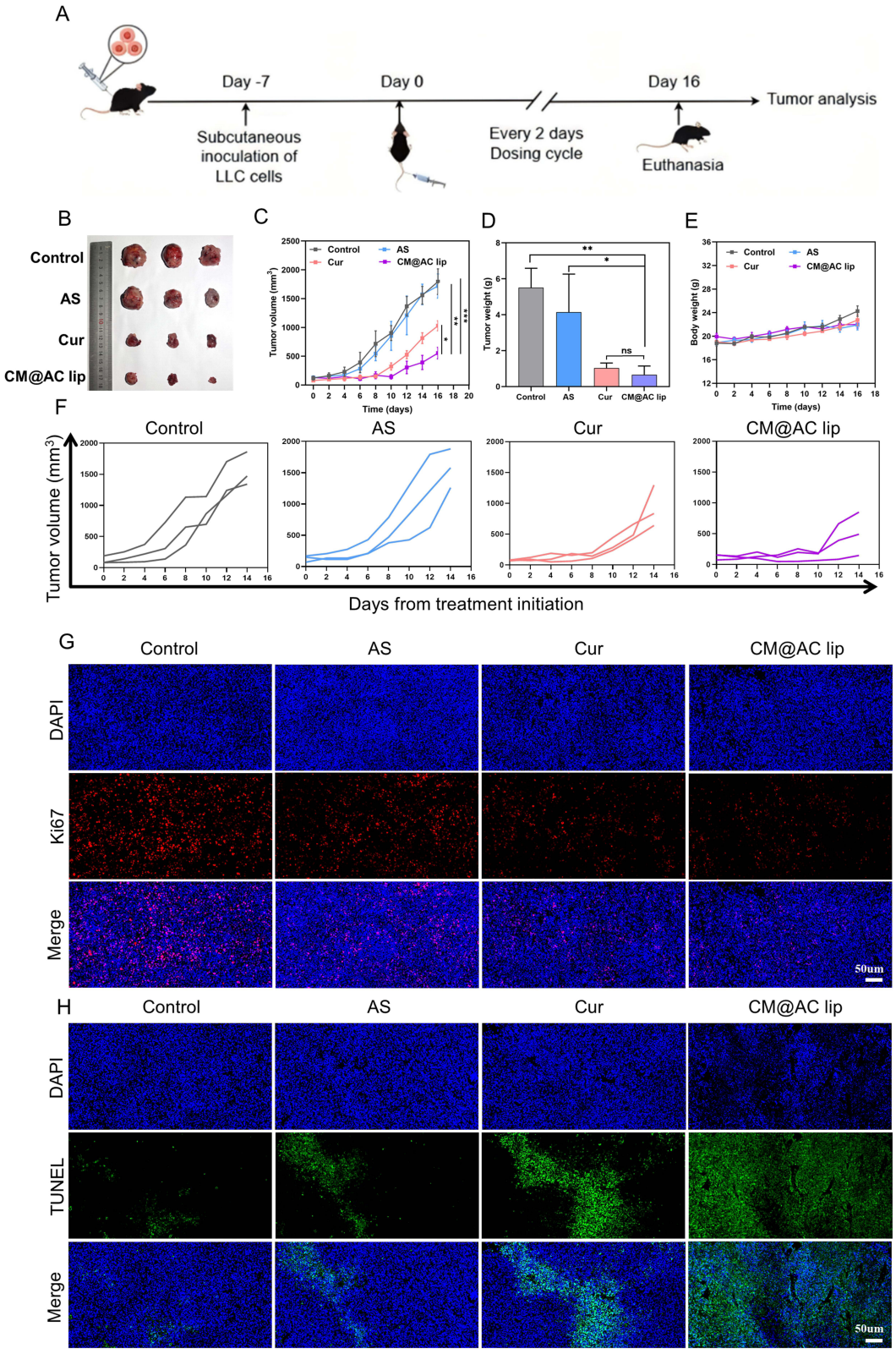

Figure 9 In vivo antitumor efficacy and biosafety evaluation of CM@AC lip. (**A**) Schematic of the in vivo treatment protocol. (**B**) Photographs of excised tumors after different treatment. (**C**) Tumor growth curves during the 14-day treatment period. (**D**) Tumor weight of different groups. (**E**) Body weight changes of mice during treatment. (**F**) Individual tumor growth curves for each mouse. (**G**) Immunofluorescence staining of Ki67 in tumor tissues (red). (**H**) Immunofluorescence staining of TUNEL in tumor tissues (green). Nuclei were counterstained with DAPI (blue), scale bar = 50 μm. All data are presented as mean ± SD (n = 3), $*p < 0.05$, $**p < 0.01$, ns: no statistical significance.

https://doi.org/10.2147/IJN.S558285

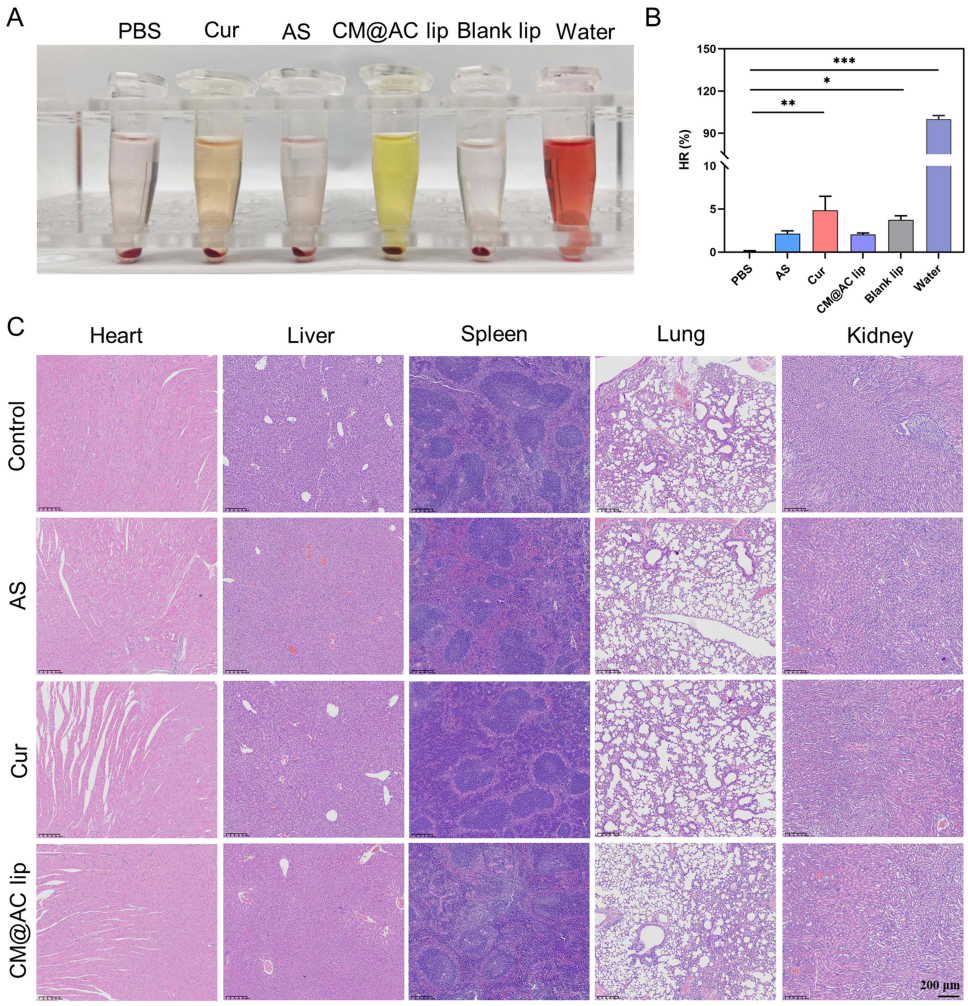

Figure 10 Biosafety evaluation of CM@AC lip. (**A**) Representative images of hemolysis after 4 h incubation of various formulations with 2% erythrocyte suspension at 37 °C. (**B**) Quantitative analysis of hemolysis rate. (**C**) H&E-stained histological sections of heart, liver, spleen, lung, kidney, Scale bar = 200 μm. All data are presented as mean ± SD (n = 3). *$p < 0.05$, **$p < 0.01$, ***$p < 0.001$.

Discussion

Combination therapy is a promising strategy for overcoming tumor heterogeneity and drug resistance by modulating multiple molecular pathways simultaneously.[34] In this study, a systematic combination index (CI) analysis was conducted to identify the optimal synergistic ratio between curcumin and astragaloside IV. This quantitative approach is widely recognized for its accuracy in evaluating drug–drug interactions in vitro, allowing us to distinguish between additive, synergistic, and antagonistic effects.[35] The CI–FA analysis demonstrated that curcumin and astragaloside IV displayed a strong synergistic cytotoxic effect at a molar ratio of 1:1.5, indicating that this ratio maximized the cooperative inhibition of lung cancer cell proliferation. This scientifically rigorous screening ensured the formulation was developed at a ratio that provided the most potent antitumor effect, thereby establishing a robust foundation for subsequent formulation optimization.

The CM@AC liposomes exhibited a negative ζ potential (−20.8 ± 3.63 mV), which is a typical characteristic of lipid-based nanocarriers containing phospholipid and PEGylated components. Although cell membranes also possess a net negative charge, such surface potential does not necessarily hinder cellular uptake. Cellular internalization of these liposomes is primarily driven by receptor-mediated endocytosis rather than by electrostatic attraction.[36] In the case of CM@AC liposomes, the tumor-derived membrane proteins facilitate homotypic recognition and promote active uptake by LLC cells, thereby overcoming electrostatic repulsion. Moreover, Furthermore, the moderate negative charge prevents

nonspecific aggregation through electrostatic repulsion, improves stability in physiological environments, and contributes to prolonged systemic circulation, consistent with the findings of Jiang et al.[37]

The cellular uptake and biodistribution studies further validated the dual functions of immune evasion and active targeting in CM@AC liposomes. Macrophage uptake of CM@Cur liposomes was markedly lower than that of free drug or conventional liposomes, and the uptake by LLC tumor cells was significantly enhanced. In vivo fluorescence imaging and ex vivo organotypic analysis also demonstrated that the CM@ICG liposome group exhibited significantly higher fluorescence intensity in tumor tissue than free ICG and ICG liposomes. This superior tumor targeting is attributed to the synergistic effects of erythrocyte membrane–mediated immune evasion and tumor membrane–mediated homotypic adhesion.[32,33] The SDS-PAGE results confirmed that CM@AC lip retained characteristic proteins from both erythrocyte and cancer cell membranes, supporting the successful hybridization that underlies these biological advantages.

Both in vitro and in vivo evaluations demonstrated that CM@AC liposomes significantly improved therapeutic performance compared with single-drug or non-coated formulations. The formulation induced stronger cytotoxicity, higher apoptotic rates, and greater inhibition of invasion in vitro, while producing the highest tumor growth inhibition rate (74.6%) in vivo. This enhanced efficacy can be attributed to several synergistic factors:: (i) the optimized 1:1.5 molar ratio that maximizes pharmacodynamic synergy between curcumin and astragaloside IV; (ii) the hybrid membrane coating that enables precise tumor targeting and efficient cellular uptake; and (iii) the sustained and pH-responsive drug release behavior of liposomes. Under acidic conditions, the ionization of phospholipid headgroups and partial protonation of curcumin and astragaloside IV weaken hydrophobic interactions and hydrogen bonding within the lipid bilayer, increasing membrane fluidity and permeability. This pH-sensitive behavior promotes preferential drug release in tumor tissues while minimizing premature leakage under physiological conditions, thereby enhancing therapeutic selectivity.

In addition to therapeutic efficacy, CM@AC liposomes exhibited excellent safety and biocompatibility. The blank liposomes showed negligible cytotoxicity toward HUVECs, maintaining cell viability above 80% even at high concentrations, confirming good compatibility with normal endothelial cells. Hemolysis assays indicated minimal erythrocyte disruption (<5%), and histopathological analysis revealed no observable organ damage or inflammatory infiltration in treated animals. Furthermore, all treatment groups maintained stable body weights throughout the experimental period, demonstrating systemic tolerance. These findings collectively indicate that CM@AC liposomes possess a favorable safety, which can be largely attributed to their tumor-targeted delivery and the responsive drug release behavior that minimizes off-target exposure.[38,39]

Conclusion

In this study, a biomimetic nanoparticle drug delivery system (CM@AC liposome) was successfully developed, utilizing a hybrid membrane of cancer cell membranes and erythrocyte membranes to co-deliver astragaloside IV and curcumin. Both in vitro and in vivo experiments demonstrated that this biomimetic system significantly enhanced the antitumor efficacy of the therapeutic agents while exhibiting excellent biosafety. The improved therapeutic performance can be attributed to the synergistic effect of the dual-drug combination and the delivery advantages conferred by the hybrid membrane: the cancer cell membrane component enables homotypic targeting, promoting selective uptake by tumor cells, while the erythrocyte membrane confers immune evasion capabilities, prolongs systemic circulation, and enhances passive tumor accumulation via the EPR effect. In conclusion, this hybrid membrane-coated delivery platform effectively improves drug targeting and therapeutic efficacy with minimal toxicity, offering promising potential for the treatment of lung cancer and other malignant tumors.

Acknowledgments

This work was funded by National Natural Science Foundation of China (82304969, 82473871, U2230123, 82304789), Sichuan Science and Technology Program (24NSFTD0024, 26ZRMS2212, 2025ZDZX0134), China Postdoctoral Science Foundation Special Funding Program (2024T170100), Chengdu Science and Technology Project (2024-YF05-01487-SN, 2026-YF09-00015-SN), and the Sichuan Provincial Medical Youth Innovation Research Project (Q21015, Q22007).

Disclosure

The authors declare no competing interest in this work.

References

1. Bray F, Laversanne M, Sung H, et al. Global cancer statistics 2022: GLOBOCAN estimates of incidence and mortality worldwide for 36 cancers in 185 countries. *CA Cancer J Clin*. 2024;74(3):229–263. doi:10.3322/caac.21834
2. Leiter A, Veluswamy RR, Wisnivesky JP. The global burden of lung cancer: current status and future trends. *Nat Rev Clin Oncol*. 2023;20(9):624–639. doi:10.1038/s41571-023-00798-3
3. Cheng W, Kang K, Zhao A, et al. Dual blockade immunotherapy targeting PD-1/PD-L1 and CTLA-4 in lung cancer. *J Hematol Oncol*. 2024;17(1):54. doi:10.1186/s13045-024-01581-2
4. Spicer JD, Cascone T, Wynes MW, et al. Neoadjuvant and adjuvant treatments for early stage resectable NSCLC: consensus recommendations from the international association for the study of lung cancer. *J Thorac Oncol*. 2024;19(10):1373–1414. doi:10.1016/j.jtho.2024.06.010
5. Steinfort DP, Kothari G, Wallace N, et al. Systematic endoscopic staging of mediastinum to guide radiotherapy planning in patients with locally advanced non-small-cell lung cancer (SEISMIC): an international, multicentre, single-arm, clinical trial. *Lancet Resp Med*. 2024;12(6):467–475. doi:10.1016/S2213-2600(24)00010-9
6. Pu L, Dhupar R, Meng X. Predicting postoperative lung cancer recurrence and survival using cox proportional hazards regression and machine learning. *Cancers*. 2024;17(1):33. doi:10.3390/cancers17010033
7. Verginadis II, Citrin DE, Ky B, et al. Radiotherapy toxicities: mechanisms, management, and future directions. *Lancet*. 2025;405(10475):338–352. doi:10.1016/S0140-6736(24)02319-5
8. Ferro A, Marinato GM, Mulargiu C, et al. The study of primary and acquired resistance to first-line osimertinib to improve the outcome of EGFR-mutated advanced non-small cell lung cancer patients: the challenge is open for new therapeutic strategies. *Crit Rev Oncol Hematol*. 2024;196:104295. doi:10.1016/j.critrevonc.2024.104295
9. Ghanbar MI, Suresh K. Pulmonary toxicity of immune checkpoint immunotherapy. *J Clin Invest*. 2024;134(2). doi:10.1172/JCI170503
10. Piha-Paul S, Olwill SA, Hamilton E, et al. A first-in-human study of cinrebafusp alfa, a HER2/4-1BB bispecific molecule, in patients with HER2-positive advanced solid malignancies. *Clin Cancer Res*. 2025;31(2):288–298. doi:10.1158/1078-0432.CCR-24-1552
11. Tang C, Liu J, Yang C, et al. Curcumin and its analogs in non-small cell lung cancer treatment: challenges and expectations. *Biomolecules*. 2022;12(11):1636. doi:10.3390/biom12111636
12. Hao M, Chu Y, Lei J, et al. Pharmacological mechanisms and clinical applications of curcumin: update. *Aging Dis*. 2023;14(3):716–749. doi:10.14336/AD.2022.1101
13. Shaikh S, Shaikh J, Naba YS, et al. Curcumin: reclaiming the lost ground against cancer resistance. *Cancer Drug Resist*. 2021;4(2):298–320. doi:10.20517/cdr.2020.92
14. Wu Q, Ou H, Shang Y, et al. Nanoscale formulations: incorporating curcumin into combination strategies for the treatment of lung cancer. *Drug Des Devel Ther*. 2021;15:2695–2709. doi:10.2147/DDDT.S311107
15. Yang ZJ, Huang SY, Zhou DD, et al. Effects and mechanisms of curcumin for the prevention and management of cancers: an updated review. *Antioxidants*. 2022;11(8):1481. doi:10.3390/antiox11081481
16. Carstens MR, Wasserfall CH, Acharya AP, et al. GRAS-microparticle microarrays identify dendritic cell tolerogenic marker-inducing formulations. *Lab Chip*. 2021;21(18):3598–3613. doi:10.1039/d1lc00096a
17. Xu F, Cui WQ, Wei Y, et al. Correction: astragaloside IV inhibits lung cancer progression and metastasis by modulating macrophage polarization through AMPK signaling. *J Exp Clin Cancer Res*. 2023;42(1):70. doi:10.1186/s13046-023-02643-y
18. Wang Y, Zhang Z, Cheng Z, et al. Astragaloside in cancer chemoprevention and therapy. *Chin Med J*. 2023;136(10):1144–1154. doi:10.1097/CM9.0000000000002661
19. Zhang Q, Yang C, Gao X, et al. Phytochemicals in regulating PD −1/ PD-L1 and immune checkpoint blockade therapy. *Phytother Res*. 2024;38(2):776–796. doi:10.1002/ptr.8082
20. Xu F, Li M, Que Z, et al. Combined chemo-immuno-photothermal therapy based on ursolic acid/astragaloside IV-loaded hyaluronic acid-modified polydopamine nanomedicine inhibiting the growth and metastasis of non-small cell lung cancer. *J Mater Chem B*. 2023;11(15):3453–3472. doi:10.1039/d2tb02328h
21. MacDonald WJ, Purcell C, Pinho-Schwermann M, et al. Heterogeneity in Cancer. *Cancers*. 2025;17(3):441. doi:10.3390/cancers17030441
22. Wang X, Bai H, Zhang JY, et al. Genetic intratumor heterogeneity remodels the immune microenvironment and induces immune evasion in brain metastasis of lung cancer. *J Thorac Oncol*. 2024;19(2):252–272. doi:10.1016/j.jtho.2023.09.276
23. Hu L-Y, Zhuang W-T, Chen M-J, et al. EGFR oncogenic mutations in NSCLC impair macrophage phagocytosis and mediate innate immune evasion through up-regulation of CD47. *J Thorac Oncol*. 2024;19(8):1186–1200. doi:10.1016/j.jtho.2024.03.019
24. Zhou C, Tang KJ, Cho BC, et al. Amivantamab plus chemotherapy in NSCLC with EGFR Exon 20 insertions. *N Engl J Med*. 2023;389(22):2039–2051. doi:10.1056/NEJMoa2306441
25. Zhong SJ, Xing YD, Dong LY, et al. Progress in the study of curcumin metabolism in vivo. *J Asian Nat Prod Res*. 2025;27(5):639–657. doi:10.1080/10286020.2024.2420619
26. Zhang H, Song J, Dai H, et al. Effects of puerarin on the pharmacokinetics of astragaloside IV in rats and its potential mechanism. *Pharm Biol*. 2020;58(1):328–332. doi:10.1080/13880209.2020.1746362
27. Wang H, Di W, Gao X, et al. Materials, syntheses and biomedical applications of nano-quercetin formulations: a comprehensive literature review. *Int J Nanomed*. 2025;20:8729–8764. doi:10.2147/IJN.S517079
28. Huang L, Huang X-H, Yang X, et al. Novel nano-drug delivery system for natural products and their application. *Pharmacol Res*. 2024;201:107100. doi:10.1016/j.phrs.2024.107100
29. Zhao LP, Zheng RR, Rao XN, et al. Chemotherapy-enabled colorectal cancer immunotherapy of self-delivery nano-PROTACs by inhibiting tumor glycolysis and avoiding adaptive immune resistance. *Adv Sci*. 2024;11(15):e2309204. doi:10.1002/advs.202309204

30. Peng J, Zhou J, Liu X, et al. A biomimetic nanocarrier facilitates glucose consumption and reactive oxide species accumulation in enzyme therapy for colorectal cancer. *J Control Release*. 2024;367:76–92. doi:10.1016/j.jconrel.2024.01.041
31. Chen S, Lan H, Liu M, et al. Less is more: biomimetic hybrid membrane nanocarriers for highly efficient tumor targeted drug delivery. *Small*. 2025;21(6):e2407245. doi:10.1002/smll.202407245
32. Xiong J, Wu M, Chen J, et al. Cancer-erythrocyte hybrid membrane-camouflaged magnetic nanoparticles with enhanced photothermal-immunotherapy for ovarian cancer. *ACS Nano*. 2021;15(12):19756–19770. doi:10.1021/acsnano.1c07180
33. Zhang W, Zhao M, Gao Y, et al. Biomimetic erythrocytes engineered drug delivery for cancer therapy. *Chem Eng J*. 2022;433:133498. doi:10.1016/j.cej.2021.133498
34. Bhat GR, Sethi I, Sadida HQ, et al. Cancer cell plasticity: from cellular, molecular, and genetic mechanisms to tumor heterogeneity and drug resistance. *Cancer Metastasis Rev*. 2024;43(1):197–228. doi:10.1007/s10555-024-10172-z
35. Chou T-C. Drug combination studies and their synergy quantification using the chou-talalay method. *Cancer Res*. 2010;70(2):440–446. doi:10.1158/0008-5472.Can-09-1947
36. Liu P, Lan S, Gao D, et al. Targeted blood-brain barrier penetration and precise imaging of infiltrative glioblastoma margins using hybrid cell membrane-coated ICG liposomes. *J Nanobiotechnol*. 2024;22(1):603. doi:10.1186/s12951-024-02870-1
37. Jiang T, Guo C, Zhang Z, et al. Biomimetic NIR-II aggregation-induced emission nanoparticles for targeted photothermal therapy of ovarian cancer. *J Mater Chem B*. 2025;13(13):4094–4102. doi:10.1039/d4tb02855d
38. Lei S, Li J, Zhu M, et al. Chimeric antigen receptor-engineered cell membrane-coated nanoparticles promote dual-targeted mRNA-based cancer gene therapy. *ACS Nano*. 2025;19(16):15668–15684. doi:10.1021/acsnano.4c18153
39. Lei W, Yang C, Wu Y, et al. Nanocarriers surface engineered with cell membranes for cancer targeted chemotherapy. *J Nanobiotechnol*. 2022;20(1):45. doi:10.1186/s12951-022-01251-w